Simple Camera Calibration via Space Angle

Dave Knopp
Stellacore Corporation

Document ID: t_QuickCal_v0r1

***Abstract*—Camera calibration is a fundamental concept in photogrammetry and computer vision applications. When working with new camera systems, it often desirable to estimate the most important calibration parameter values reliably and easily without the need for special calibration items or application software. This technical note describes a simple and practical technique for determining the "principal" camera calibration values using a single image exposure and three scene distance measurements. The associated calibration process can be completed in a few minutes time and requires only simple algebraic computations easily performed with a common calculator or spreadsheet application. The technique's simplicity and effectiveness are demonstrated by estimating the principal distance for a smart phone camera. The obtained calibration results are validated by using them to perform simple three-dimensional (3D) object reconstruction operations using an independently acquired pair of images from the same camera. Evaluation of calibration data precision and independent assessment of the subsequent reconstruction test results both indicate that the proposed method is effective.**

***Index Terms*—Photogrammetry, Computer Vision, Camera Calibration**

I. Introduction

A. Background

Camera calibration is a concept that is fundamental in the formulation of photogrammetry and computer vision applications. The calibration model may be expressed implicitly as part of a more general image formation mathematical model or the camera may be represented explicitly by its own math model. In the later case, it is common to utilize a calibration process to determine specific numeric values for the various parameters in the explicit camera model.

Camera models range from simple to sophisticated. Sometimes, a simple model is completely sufficient for a particular applications. At other times, a simple model is useful for exploratory design/simulation work or as initial values for computational processes that compute more sophisticated models using iterative refinement techniques.

The vast majority of common camera systems, at their most fundamental level, behave like a simple camera obscura[1]. In this context, the camera construction includes a small aperture (e.g. within the lens assembly) that is located some distance in front of a geometrically flat image plane. This simple geometry is only an approximation for real camera systems.

Even for advanced applications employing sophisticated camera models, it is frequently useful to quickly estimate the basic camera properties using a simple pinhole model. Also, it is often convenient if the computations can be done with simple algebra and arithmetic so that results can be computed with a simple calculator or spreadsheet application without having to resort to complex data fitting tools and processes.

[1]Historically, a camera obscura is associated with a darkened room inside of which an observer sits. The room is light tight with the exception of a small hole in one wall that emits light from an outdoor scene. Light entering the room though this hole strikes the far wall of the room and produces a faint (inverted) image observable by the person inside - cf. https://en.wikipedia.org/wiki/Camera_obscura

B. Approach

The simple method, described herein, allows recovering the camera principal distance given only two detector image position measurements and a known object space angle which can be determined quickly and easily with three distance measurements. The overall calibration process can be completed in a few minutes time requiring only simple algebraic computations that can be performed easily with an arithmetic calculator or spreadsheet application.

The derivation provides an algebraic expression for principal distance value in terms of the roots of quadratic equations. When the geometric configuration is sufficient to determine a unique physical solution, the presented method provides a unique solution. For weak geometric configurations, two physically meaningful solutions are possible for which the described method provides both.

The technique is valid for cameras with optical systems that approximate rectilinear image formation: i.e. for "normal" optical system designs with relatively low distortion characteristics. The pinhole perspective model often provide reasonable results for the majority of typical consumer devices, surveillance cameras, and industrial monitoring systems. The simple pinhole model can be expected to breakdown for super- and ultra-wide angle and fish-eye optics.

The simplicity and effectiveness of the technique are demonstrated by describing calibration of a smart phone camera by measuring two features on a single image and recording three object distances measured with a retractable steel tape. The validity of the obtained camera calibration is assessed by computing a classic three-dimensional (3D) coordinate reconstruction from a pair of additional photographs taken with the same camera.

II. Methodology

A. Camera Concepts

The geometric characteristics of a camera obscura (aka "pinhole camera", "central perspective projection camera") are concerned with the location of the light admitting aperture relative to the plane on which the image is formed.

For a typical modern camera, the image plane is the surface of a light sensitive semi-conductor devics (generally a CMOS or CCD). The detector cells (aka "pixels") on the device form

a natural coordinate system, in terms of "row" and "column" directions. For modern manufacturing techniques, the surface of the detector is highly isotropic with equal and uniform pixel spacing in both row and column directions. In addition, the detector surface is generally very flat and may be considered planar. Thus, the physical detector construction itself provides a natural two-dimensional (2D) Cartesian coordinate frame.

The 2D detector coordinates can be extended mathematically into a three-dimensional (3D) Cartesian coordinate frame. This is done by defining a direction that is orthogonal to both the row and column directions on the detector and associated with the same units of measurement. By convention herein, this third axis is positive outward from the detector surface.

The 3D coordinate frame tied to the detector is the camera's "interior" coordinate frame. The simple "pinhole-model" camera calibration is associated by the location of the entrance aperture. This location may be represented as a vector that is expressed in the camera's interior detector coordinate frame.

B. Mathematics Formulation

The mathematical formulation below touches on a few concepts from geometric algebra (GA) [1], [4] including use of simple algebraic operations to manipulate vectors, and suggesting that the optical angles are better represented as bivector entities. However, the fundamental operations and results are easily understood in terms of real algebra and basic plane trigonometry.

The notation employed herein follows that of Hestenes [1], in which scalars are represented with lower case Greek letters, vectors with lower case Roman letters, and bivectors with upper case Roman letters.

Geometric concepts are expressed in terms of the relationship between two coordinate systems:

- Ref An arbitrary "Reference" coordinate frame (e.g an "object space" or "world frame")
- Det The "Detector" surface of an image sensor associated with the camera (e.g. the coordinate frame associated with a CMOS or CCD array)

For computational purposes, each of these coordinate system can be associated with a collection of mutually orthogonal, dextral, unit basis vectors denoted as $\{e_1, e_2, e_3\}$.

C. Simple Camera Model

For ideal central perspective image formation a camera model can be associated with the following conditions representing extreme limit cases of a more general model such as in [2], [3]. For the simple "pinhole" camera model,

1) Entrance pupil may be approximated as a point with location that is fixed relative to the optical system (and camera body)
2) Exit angle equals entrance angle (i.e. assume no distortion or other aberrations)
3) Exit pupil is approximated as a point with location fixed relative to the optical system (and camera body)
4) Detector is positioned such that the boundary of its active surface is centered on the optical system exit axis and the (assumed to be planar) sensor surface is orthogonal to the exit axis.

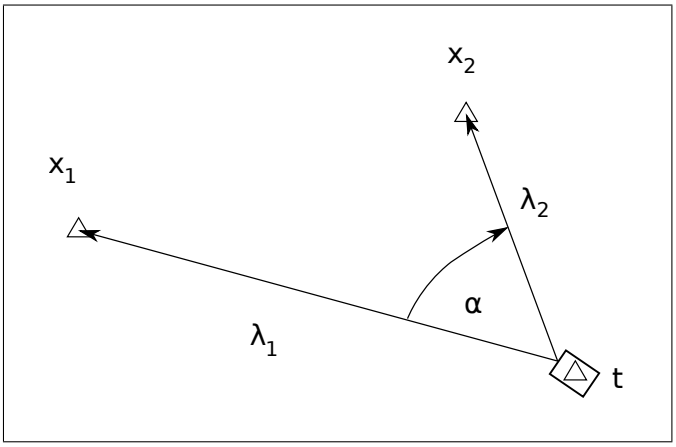

Figure 1. Exterior space angle, $\alpha = |A|$, defined by two object points at x_1 and x_2 relative to camera station at t. The camera station is the location of the optical system entrance pupil as expressed in the exterior reference frame.

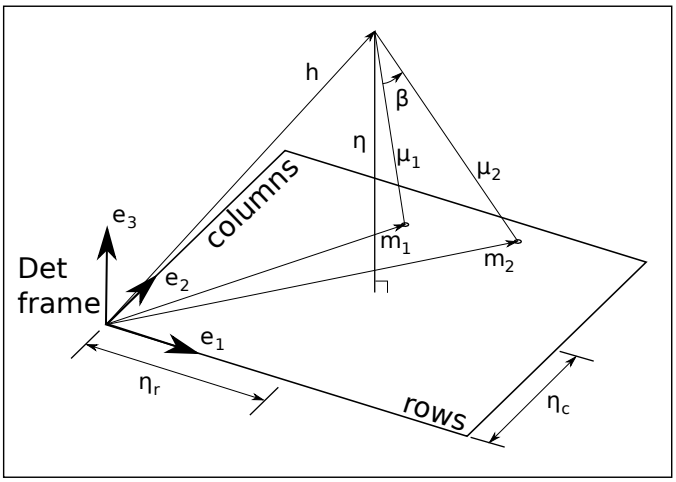

Figure 2. Interior space angle defined by two detector locations, m_1 and m_2, relative to optical system exit pupil at location, h, expressed in the detector reference frame. The detector locations are a distance, μ_1 and μ_2 from the pupil, subtend the angle, $\beta = |B|$.

D. Geometric Configuration

Referring to figure 1, let vector, t, represent the location of the entrance pupil as it is expressed in the Ref frame, and let vectors, x_1 and x_2, represent two arbitrary but distinct locations with values expressed also in the Ref frame. Denote the target range distances from t to x_1 and x_2, by respective scalar values, λ_1 and λ_2, defined for $j = 1, 2$, as

$$\lambda_j \equiv |x_j - t| = \sqrt{(x_j - t)^2} \tag{1}$$

Let bivector, A, represent the entrance angle, and bivector, B, represent the exit angle. The distortion free model is represented as the identity relationship, $B = A$. However, since the 3D nature of the angle geometry is not needed herein,

introduce scalar values, α and β, to represent the entrance and exit angle magnitudes

$$\alpha \equiv |A|$$
$$\beta \equiv |B|$$

and express the central perspective condition as (ref. section II-C assumption 2)

$$\beta = \alpha \tag{2}$$

Let vector, h, known as the "principal vector[2]", represent the location of the exit pupil as it is expressed in the Det frame. Also let vectors, m_1 and m_2, represent two image locations expressed in the Det frame, while scalar values, μ_1 and μ_2, represent the respective magnitudes,

$$\mu_j \equiv |m_j - h| = \sqrt{(m_j - h)^2} \tag{3}$$

These relationships are illustrated in figure 2.

The detector positioning relationship relative to the optical system exit axis (ref. section II-C assumption 4) may be summarized by expressing the principal vector, h, relative to an orthonormal vector basis associated for the detector, via

$$h = \eta_r e_1 + \eta_c e_2 + \eta e_3$$

where the scalar value components, η_r, and η_c, respectively represent the row and column location of the principal point (of autocollimation) and the scalar value η is the principal distance value of present interest (cf. figure 2).

1) Parameter Domains: The λ_j represent physical distances and therefore expected to be non-negative. In addition, the object point locations should not be coincident with the camera station, so that

$$0 < \lambda_j$$

Similar arguments apply to the intrinsic distances, μ_j, so that also,

$$0 < \mu_j$$

The principal distance, η, may also be required to be non-negative (by appropriate selection of detector frame conventions). It should also be non-zero to avoid degenerate imaging geometry, so that,

$$0 < \eta$$

For the ideal case of central perspective projection onto a flat, and finite, image surface, the exit angle is limited in magnitude[3]. By virtue of the distortion free condition, the entrance angle is correspondingly limited. This condition may be expressed as

$$(|\alpha| = |\beta|) < \frac{\pi}{2}$$

In particular, this means that the cosine cannot assume a negative value. A more stringent condition may be expressed as,

$$0 < (\cos\alpha = \cos\beta) < 1 \tag{4}$$

in which the left hard inequality requires also avoiding the zero-angle condition associated with a physical configuration in which object locations, x_1, x_2 and t are collinear.

2) Detector-Axis Relationship: Since the detector surface is assumed flat, the measurement vectors, m_j, must lie in the plane of the detector which itself is orthogonal to the optical exit axis. For exit axis aligned with the e_3 basis vector, this means that,

$$m_j \cdot e_3 = 0$$

Therefore,

$$m_j \cdot h = m_{jr}\eta_r + m_{jc}\eta_c$$

where m_{jr} and m_{jc} are, respectively, the row and column components of the measured detector position for the j-th point.

For the simple camera model in use here, the principal point components, η_r and η_c, are fixed (at the center of the detector) and readily known in terms of the overall image size. Therefore, given a specific measurement, m_j, for a location on the detector, the value of $m_j \cdot h$, is completely determined. In particular, for this assumed simple camera model, the scalar value, $m_j \cdot h$, is entirely independent of the principal distance, η.

Represent this measurement construct with scalar value, ρ_j^2, defined in terms of detector row and column location measurements, as

$$\rho_j^2 \equiv m_j \cdot h$$

which may be expanded,

$$\rho_j^2 = m_{jr}\eta_r + m_{jc}\eta_c \tag{5}$$

E. Angularity Relationships

1) Entrance Angle Magnitude: Introduce vector, d, to represent the object point separation via definition,

$$d \equiv x_2 - x_1$$

and square each side of this relationship to obtain,

$$d^2 = x_2^2 - 2x_2 \cdot x_1 + x_1^2$$

[2]As the term is used herein, the principal vector, h, may be decomposed as a sum of two vector constituents. The first constituent lies in the plane of the detector and has two components that represent the location of the "principal point" (of autocollimation). The second constituent is the component of h perpendicular to the detector surface. The magnitude of this orthogonal component is known as the "principal distance". For the special case in which a camera is focused at infinity, the principal distance is approximately equal to the optical system focal length. However, in general the principal distance has a somewhat abstract interpretation. Its numeric value is determined as a "best fit" to the pinhole central perspective model and therefore may be affected by other considerations (various high order optical effects and aberrations).

[3]This is a limitation of the pinhole / central perspective projection model and not a limitation of actual optical systems. Physical lenses exist with larger than 180-deg full field of view. The fact that real optical systems exceed this limit, demonstrates that the simple perspective projection model, at best, is a simplifying approximation only valid for a restricted subset of actual optical systems. In general, validity of the approximation improves for increasingly more telephoto optical systems, and degrades with increasingly wider angle ones. The central perspective model fails completely for substantially non-rectilinear designs such as super-wide, ultra-wide angle, fish-eye and other extreme optical systems.

Simultaneously, the entry angle magnitude, α, satisfies the Ref space triangle law of cosines relationship, via

$$d^2 = \lambda_1^2 + \lambda_2^2 - 2\lambda_1\lambda_2 \cos\alpha$$

which may also be expressed,

$$\cos\alpha = \frac{\lambda_1^2 + \lambda_2^2 - d^2}{2\lambda_1\lambda_2} \tag{6}$$

2) Exit Angle Magnitude: In similar fashion, let the relative detector point separation be represented by vector, r, defined as

$$r \equiv m_2 - m_1$$

and square each side to obtain,

$$r^2 = m_2^2 - 2m_2 \cdot m_1 + m_1^2 \tag{7}$$

The exit angle magnitude, β, satisfies the corresponding vertex magnitude relationship via the law of cosines,

$$r^2 = \mu_1^2 + \mu_2^2 - 2\mu_1\mu_2 \cos\beta$$

or, as

$$\cos\beta = \frac{\mu_1^2 + \mu_2^2 - r^2}{2\mu_1\mu_2} \tag{8}$$

3) Coangularity Condition: The ideal perspective condition may be expressed as $\beta = \alpha$, which also requires that

$$\cos\beta = \cos\alpha$$

This equivalence may be expressed in terms of the above triangle relationships from equation 6 and 8,

$$\frac{\lambda_1^2 + \lambda_2^2 - d^2}{\lambda_1\lambda_2} = \frac{\mu_1^2 + \mu_2^2 - r^2}{\mu_1\mu_2}$$

The left hand side, may be evaluated in terms of measured object space distances, while evaluation of the right hand side requires knowledge of camera interior parameters including the principal distance.

For convenience of notation, introduce a new scalar parameter, γ, that is proportional to the common value in this equivalence. For calibration purposes, it is particularly useful to associate γ more closely with the object space quantity on the left and to *define* the parameter, γ, as

$$\gamma \equiv \frac{\lambda_1^2 + \lambda_2^2 - d^2}{\lambda_1\lambda_2} = 2\cos\beta$$

This allows expressing the coangularity condition as

$$\mu_1\mu_2\gamma = \mu_1^2 + \mu_2^2 - r^2 \tag{9}$$

4) Squared Relationships: Square both sides of equation 9 to obtain

$$\mu_1^2\mu_2^2\gamma^2 = \left(\mu_1^2 + \mu_2^2\right)^2 - 2\left(\mu_1^2 + \mu_2^2\right)r^2 + r^4 \tag{10}$$

Since both the μ_j and r^2 are inherently positive, squaring these quantities does not significantly change the underlying relationship. However, since γ can be either positive or negative, the squaring operation conflates two cases and thereby introduces a possible secondary solution.

I.e. this squared relationship, still represents the true physical configuration associated with $\gamma = 2\cos\beta$, but the squaring operation also introduces an artificial solution associated with the vertex angle supplement, $-\gamma = 2\cos(\pi - \beta)$. Thus, any inversion process to determine, η, should be expected to require also a disambiguation consideration.

To evaluate this relationship in terms of the (unknown) principal distance parameter, begin by squaring both sides of equation 3 to obtain

$$\begin{aligned}\mu_j^2 &= (m_j - h)^2 \\ &= m_j^2 - (m_j h + h m_j) + h^2 \\ &= m_j^2 - 2m_j \cdot h + h^2\end{aligned}$$

The middle term on the right may be expressed in terms of relationship 5, so that

$$\mu_j^2 = m_j^2 - 2\rho_j^2 + h^2 \tag{11}$$

Employ this interior distance relationship for each point to express the product

$$\mu_1^2\mu_2^2 = \left(\left(m_1^2 - 2\rho_1^2\right) + h^2\right)\left(\left(m_2^2 - 2\rho_2^2\right) + h^2\right)$$

Distribute the multiplications to yield

$$\begin{aligned}\mu_1^2\mu_2^2 = h^4 &\\ &+ \left[m_1^2 + m_2^2 - 2\left(\rho_1^2 + \rho_2^2\right)\right]h^2 \\ &+ \left[\left(m_1^2 - 2\rho_1^2\right)\left(m_2^2 - 2\rho_2^2\right)\right]\end{aligned}$$

Introduce intermediate scalar, ν^2, defined as,

$$\nu^2 \equiv \frac{1}{2}\left(m_1^2 + m_2^2\right) - \left(\rho_1^2 + \rho_2^2\right) \tag{12}$$

and scalar, ω^4, defined as

$$\omega^4 \equiv \left(m_1^2 - 2\rho_1^2\right)\left(m_2^2 - 2\rho_2^2\right)$$

to express the product of squared interior distance values as,

$$\mu_1^2\mu_2^2 = h^4 + 2\nu^2h^2 + \omega^4 \tag{13}$$

Note that the exponents included in the expression of quantities, ν^2 and ω^4, are used primarily to track the algebraic order with which they are defined. In this way, equations are expressed with notation in which terms have homogeneous order. The numeric values associated to the quantities, ν^2 and ω^4, may be negative. However, this is not a concern since not roots of these values are required.

As a next step in relating equation 10 to principal distance parameters, express the sum of squared interior distance values by adding equation 11 for the two cases of $j = 1, 2$ to yield

$$\left(\mu_1^2 + \mu_2^2\right) = m_1^2 + m_2^2 - 2\left(\rho_1^2 + \rho_2^2\right) + 2h^2$$

This may be expressed in terms of intermediate parameter, ν^2, as

$$\left(\mu_1^2 + \mu_2^2\right) = 2\left(\nu^2 + h^2\right) \tag{14}$$

Next, square this relationship to obtain,

$$\left(\mu_1^2 + \mu_2^2\right)^2 = 4\left(\nu^4 + 2\nu^2h^2 + h^4\right) \tag{15}$$

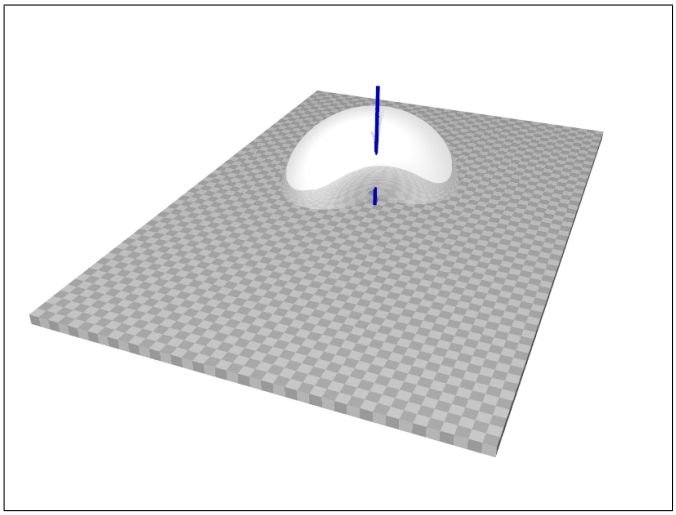

Figure 3. Perspective representation of example toroidal surface determined by two detector locations and the exit angle magnitude. The checkerboard represents the detector surface, while the blue cylinder is the optical system exit axis which, for simple camera here, is assumed to be orthogonal to the detector surface. Compare with figure 4 (left) which illustrates the cross section view in plane of detector surface. This represents one the "four-solutions" cases with two solutions above and two (not visible here) below the detector surface.3

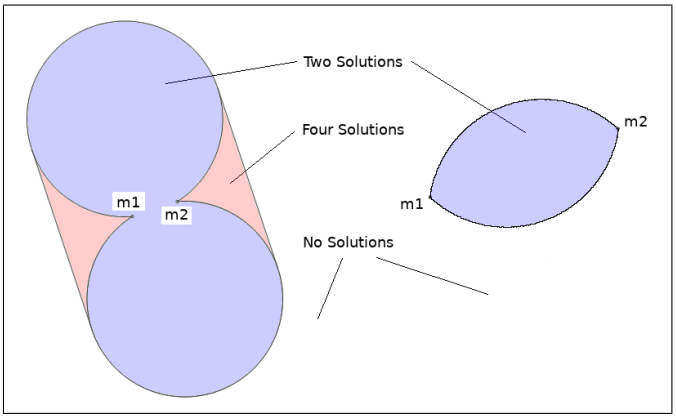

Figure 4. Domains for solution values, $\check{h}^2_{\pm}$. Detector-plane cross section view of the toroidal solution surface. The line segment between points m_1 and m_2 form the axis of revolution about which a circle arc is revolved. The (poloidal) radius of the arc is defined by locus of detector locations from which points m_1 and m_2 subtend angle β. The two solution domain correspond with the principal point being inside the torus such that the optical axis pierces the torus only twice (once above and once below the detector plane). The four-solution domains correspond to the principal point being outside the torus (cf. figure 3), while the optical axis enters and leaves the torus volume both above and below the detector surface. The case on the left corresponds with an accute angle, β, while the case on the right corresponds with an obtuse angle β.

5) Return to Coangularity: Substitute equations 13, 15 and 14, to re-express relationship 10 as,

$$\begin{aligned}\left(h^4+2\nu^2h^2+\omega^4\right)\gamma^2 = 4\left(\nu^4+2\nu^2h^2+h^4\right)\\ -4\left(\nu^2+h^2\right)r^2\\ +r^4\end{aligned}$$

Rearrange and gather terms by order of h,

$$\begin{aligned}0 = &\left(4-\gamma^2\right)h^4\\ &+\left(8\nu^2-2\nu^2\gamma^2-4r^2\right)h^2\\ &+\left(4\nu^4-4\nu^2r^2+r^4-\omega^4\gamma^2\right)\end{aligned}$$

This is a quadratic expression in terms of h^2, for which all the coefficients are completely established in terms of measured values. I.e.

$$\kappa_a h^4 + 2\kappa_b h^2 + \kappa_c = 0 \tag{16}$$

where

$$\begin{aligned}\kappa_a &\equiv 4-\gamma^2\\ \kappa_b &\equiv 4\nu^2-\nu^2\gamma^2-2r^2\\ \kappa_c &\equiv 4\nu^4-4\nu^2r^2+r^4-\omega^4\gamma^2\end{aligned}$$

Two candidate solution values, $\check{h}^2_{\pm}$, may be computed immediately from the quadratic formula. I.e.,

$$\check{h}^2_{\pm} = -\frac{\kappa_b}{\kappa_a} \pm \sqrt{\left(\frac{\kappa_b}{\kappa_a}\right)^2 - \frac{\kappa_c}{\kappa_a}}$$

with,

$$\begin{aligned}\frac{\kappa_b}{\kappa_a} &= \frac{4\nu^2-\nu^2\gamma^2-2r^2}{4-\gamma^2}\\ \frac{\kappa_c}{\kappa_a} &= \frac{4\nu^4-4\nu^2r^2+r^4-\omega^4\gamma^2}{4-\gamma^2}\end{aligned}$$

If there are two real positive solutions, then the two values of $\check{h}^2_{\pm}$ will subsequently produce two solutions that are slightly closer or further from the detector. These situation can be understood geometrically as the intersection of the optical axis with a toroid of revolution as visualized in figure 3 with a detector plane cross-section diagramed in figure 4. In the case of dual solutions, additional information is needed to select which of the $\check{h}^2_{\pm}$ solutions is appropriate to the application at hand.

For a given solution, $\check{h}^2$, representing one of the $\check{h}^2_{\pm}$, equation 16 may be expanded and rearranged to obtain an expression for γ^2 in terms of $\check{h}^2$, as

$$\gamma^2 = \frac{\left(2\check{h}^2+\left(2\nu^2-r^2\right)\right)^2}{\check{h}^4+2\nu^2\check{h}^2+\omega^4}$$

The two roots, $\gamma_{\pm} = \pm\sqrt{\gamma^2}$, correspond to a pair of supplementary angles, $\beta_{\pm}$, via

$$\begin{aligned}\gamma &= 2\cos\beta_+\\ -\gamma &= 2\cos\left(\pi-\beta_-\right)\end{aligned}$$

To obtain a solution for principal vector, h, note that

$$h^2 = \eta_r^2+\eta_c^2+\eta^2$$

so that

$$\eta = \sqrt{\check{h}^2_{\pm}-\eta_r^2-\eta_c^2}$$

Here, only the positive root is relevant based on physical considerations (the negative solution corresponds with optical system "behind" the detector).

a) Special Case - Single Solution: For the case of one solution (above the detector), the discriminant, $\left(\kappa_b^2 - 4\kappa_a\kappa_c\right)$, should be zero, and therefore, the single root is associated with,

$$\check{h}^2 = -\frac{\kappa_b}{\kappa_a}$$

which may be expressed as

$$\check{h}^2 = \frac{-4\nu^2 + \nu^2\gamma^2 + 2r^2}{4 - \gamma^2}$$

F. Computational Summary

The preceding developments and equations may be summarized as a computational recipe:

- Use detector size width and height to determine the row and column coordinates of the detector center (η_r, η_c) expressed in terms of interior with values expressed in Det units (e.g. [pix]). For the current simplified camera model, this location represents the (assumed) principal point of autocolimation.
- Establish the inter-point distance, $\sqrt{d^2}$, and range from station distances, λ_1, and λ_2 with values expressed in [Ref] units.
  - One approach is to measure the distances, $\sqrt{d^2}$, λ_1 and λ_2, directly (e.g. via steel tape measure or laser range finder)
  - An alternative is to use survey techniques (e.g. via GNSS) to establish 3D Ref frame coordinates for camera station vector, t, and the two object point vectors, x_1 and x_2, then compute distances via,

$$d^2 = (x_2 - x_1)^2$$
$$\lambda_j = \sqrt{(x_j - t)^2}$$

  - Another approach is to observe the object space angle directly by acquiring an image with camera positioned at the vertex of an object with known apex angle (e.g. from top of a gravel pile having a known angle of repose).
- Obtain, m_1 and m_2, by directly measuring the two image points of interest in Det frame coordinates (e.g. [pix] units). Use these values to compute intermediate parameters
  - Compute observation parameter reductions,

$$\gamma = \frac{\lambda_1^2 + \lambda_2^2 - d^2}{2\lambda_1\lambda_2}$$
$$r^2 = (m_2 - m_1)^2$$
$$\rho_j^2 = m_{jr}\eta_r + m_{jc}\eta_c$$

  - Then, compute intermediate parameter values

$$\nu^2 = m_1^2 + m_2^2 - 2\left(\rho_1^2 + \rho_2^2\right)$$
$$\omega^4 = \left(m_1^2 - 2\rho_1^2\right)\left(m_2^2 - 2\rho_2^2\right)$$
$$\left(\nu^2 - r^2\right) = 2\left((m_2 \cdot m_1) - \left(\rho_1^2 + \rho_2^2\right)\right)$$

Figure 5. Source photo after simple edge-detection to emphasize features of interest around the door frame. Barely visible as the featureless region to left side of image is the stairway rail having top end near left edge (about 1/3 way from top_ and bottom end appearing near (and occluding) the lower left corner of the door frame. The camera lens was held close to the top corner of the rail as practical.

  - Use these to evaluate quadratic coefficients

$$\kappa_a \equiv 4 - \gamma^2$$
$$\kappa_b \equiv 2\left(\nu^2 - r^2\right) - \frac{1}{2}\nu^2\gamma^2$$
$$\kappa_c \equiv \left(\nu^2 - r^2\right)^2 - \omega^4\gamma^2$$

- Solve the quadratic to obtain intermediate root candidates via the general quadratic formula[4],

$$\check{h}_\pm^2 = \frac{-\kappa_b \pm \sqrt{\kappa_b^2 - \kappa_a\kappa_c}}{\kappa_a}$$

  If there are two (real valued) solutions, additional information is needed to resolve which of the $\pm$ expressions to use.
- As a last step, estimate the principal distance value(s) via,

$$\eta = \sqrt{\check{h}_\pm^2 - \eta_r^2 - \eta_c^2}$$

III. Results

A. Formula Verification

The recipe and formulae described in the previous section have been implemented in a computer program and verified with simulated numeric data. The simulation results (not presented here) verify that the various formulae are correct.

B. Real Photo Calibration

To assess the method with actual imagery, a photo was acquired from a smart phone camera looking down a short flight of stairs and capturing the corners of a standard door. The camera lens was held close to the corner of the rail on the stairs in order to provide an easily identified camera

Table I
DETECTOR SIZE CHARACTERISTICS

	Value [pix]
Format	3120 x 4160
η_r	1560
η_c	2080

Table II
IMAGE FEATURE MEASUREMENTS

	(row,col) [pix]	Uncertainty [pix]
m_1	$(162., 2683.)$	5.
m_2	$(2542., 1739.)$	5.

station location. Figure 5 shows the source photo after image processing to emphasize edge features of calibration relevance.

The camera detector properties are summarized in table I.

Distances were measured using a standard retractable steel tape. The measured distances correspond to those indicated by the annotations in figure 6:

- λ_{TL} Distance from rail corner (camera station) to top left (TL) corner of door frame
- λ_{BR} Distance from rail corner (camera station) to bottom right (BR) corner of door frame
- $|d_D|$ Distance along diagonal of door frame

Measured values presented in table III along with approximate measurement uncertainty estimates. The corresponding image features were measured by recording detector row and column locations as presented in table II.

With this experiment configuration, the object space diagonal, d, traces a line that crossing the image format near the detector center with one end on either side of the center. This is a particularly strong geometry for calibration. Indeed the solution process returns only one valid root which is well defined.

Using the measurements from table III and II in the formulae of section II-F produces a principal distance estimated value,

$$\eta = 3112 \text{ [pix]}$$

Uncertainty in this value may be estimated numerically. A simple Monty Carlo style simulation using the same geometric configuration as for the observed data allows assessing the overall solution sensitivity and precision. The simulation includes two cases, "A" and case "B", associated with different magnitudes of pseudo-random error.

Simulation case "A" is computed with values representative of the actual measurement errors associated with the trial

[4]The quadratic formula may be expressed in various forms with different numeric stability properties depending on specific data values.

Table III
OBJECT DISTANCE MEASUREMENTS

Distance	Best [cm]	-Uncertainty	+Uncertainty
λ_{TL}	238.	$-.0$	$+1.$
λ_{BR}	328.	$-.0$	$+1.$
$\sqrt{d_D^2}$	230.	$-.5$	$+.5$

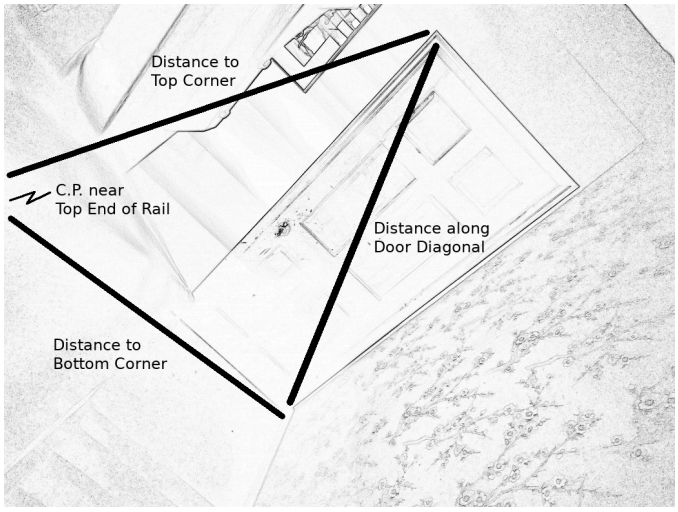

Figure 6. Annotation on top of (edge detect) image to identify which object distances are measured. The camera was held with lens entrance near top of stair rail at left edge of image. The object point range distances to top and bottom of door are indicated as is the door diagonal used for computations.

Table IV
VALUES USED FOR MONTY CARLO SIMULATION

Parameter	Mean	1-Sigma-A	1-Sigma-B
	(row,col) [pix]	[pix]	[pix]
m_1	$(162., 2683.)$	5.	1.
m_2	$(2542., 1739.)$	5.	1.
	[cm]	[cm]	[cm]
λ_{TL}	238.5	.75	.3
λ_{BR}	328.5	.75	.3
$\sqrt{d_D^2}$	230.	.5	.3

measurement process conducted hastily without great care. The error model for simulation case "B" is more typical of what can be expected when measurements are completed with reasonable care.

For the Monty Carlo simulation, the measurements are represented by samples drawn from pseudo-random normal probability distributions configured with the mean and dispersion values presented in table IV. The resulting principal distance distributions are presented in figures 7 and 8.

The precision estimate, computed using actual experiment uncertainties, indicates a standard uncertainty a bit better than 15 pixels. Given the principal distance value of about 3100 pixels, this is a relative precision on the order of

$$\frac{\sigma_\eta}{\eta} \simeq .5\,\%$$

or about one part in 200.

C. 3D Object Measurement Validation

Although the camera calibration results discussed above are consistent with expectation, it's useful to check the calibration with an independent process. To this end, the same smartphone camera was utilized in a simple 3D (three-dimensional) object reconstruction (aka structure from motion) project.

The results of the photogrammetric reconstruction (using the camera calibration described above) are compared with independent field measurements acquired with a retractable steel

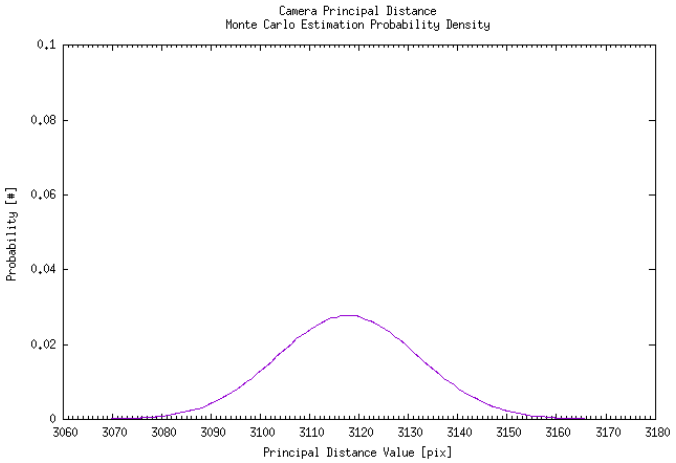

Figure 7. Distribution of principal distance values for simulation case "A" representing the actual test case including relatively careless measurement gathering. The mean and 1-sigma values for a normal distribution fit are 3117.7 and 14.4 [pix].

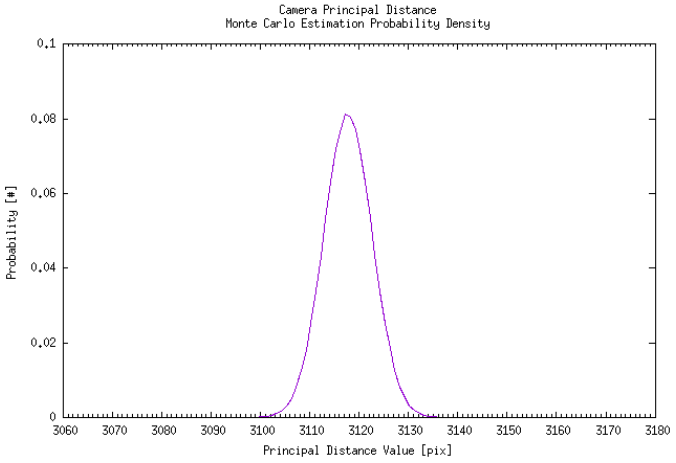

Figure 8. Distribution of principal distance values for simulation case "B" representing a hypothetical situation in which reasonable care is taken during measuring operations. The mean and 1-sigma values for a normal curve fit are 3117.7 and 4.9 [pix].

tape. This comparison provides an independent assessment of the quality of the calibration, since the validation imagery, validation image feature measurements and the reconstruction processing software are distinct from that used in the calibration process.

The validation project consists of the following steps:

1) Acquire and measure imagery. Collected here as a classic "convergent stereo pair" configuration. Measure row/column locations for various (arbitrary) corresponding image feature locations in each image of the pair.
2) Compute a "relative orientation" (RO) relationship between the two image exposures (using available custom software). Treat camera as a "metric camera" using the camera model with values as determined in section III-B and estimate values for the five parameters representing general RO degrees of freedom. Compute 3D point coordinates via space intersection using the RO solution. At

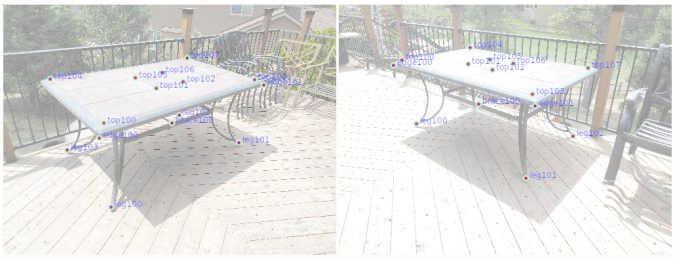

Figure 9. Stereo pair used for 3D object geometry reconstruction. The indicated image features, in conjunction with the camera calibration determined in section III-B, were utilized to compute a 3D stereo module using a standard relative orientation algorithm.

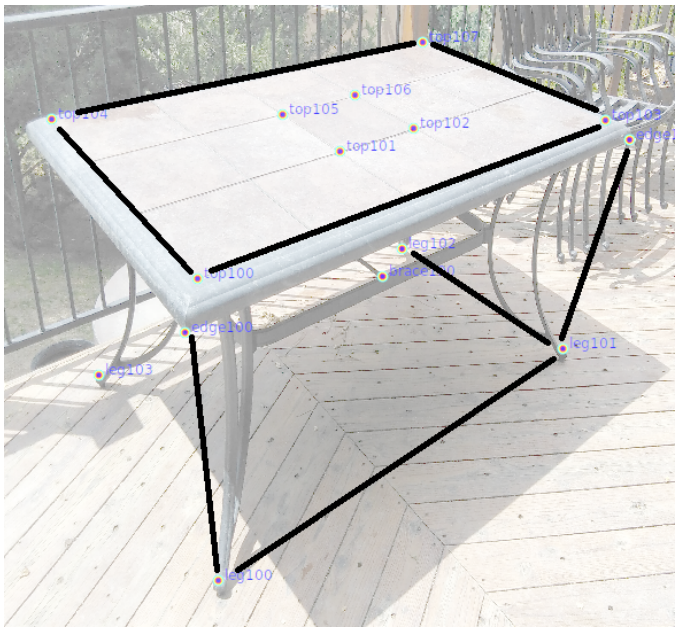

Figure 10. Check distances used to assess 3D object reconstruction quality. The heavy lines identify the individual pairs of 3D points used to define check distances.

Pnt1	Pnt2	Model Distance [mu]		[m]	Ref Dist [m]	Resid [m]
edge100	leg100	0.229	=	0.660	0.65	0.010
edge101	leg101	0.227	=	0.655	0.65	0.005
leg100	leg101	0.517	=	1.491	1.495	−0.004
leg101	leg102	0.317	=	0.914	0.925	−0.011
top100	top103	0.527	=	1.520	1.535	−0.015
top100	top104	0.322	=	0.929	0.915	0.014
top103	top107	0.316	=	0.911	0.915	−0.004
top104	top107	0.529	=	1.525	1.535	−0.010
					AbsDev:	0.009

Figure 11. Residual erros in object reconstruction associated with the check distances identified in annotation of figure 10. The model distances are computed by relative orientation algorithm and expressed in an arbitrary coordinate frame and "model units [mu]". A scale factor (computed using a single measurement of one diagonal across he table top) is applied to express distances in meters in the second "Model Distance" column. The "Ref Dist" values were measured using a retractable steel tape. The "Resid" column displays residual values (RefDist less ModelDist). The summary "AbsDev" value (i.e. 9 millimeters) is the average absolute deviation of the residuals and is entirely consistent with the a prior uncertainty of object distance measurements utilized during camera calibration (cf. table III).

this point all 3D model points are expressed in arbitrary "model units" or "[mu]" (the model scale is determined such that stereo baseline is exactly one [mu]).

3) Compute a model scale factor. Measure one of the table top diagonals (top103 to top104) using the steel tape to obtain the diagonal in Ref units (of meters). Compute scale factor as ratio of the Ref distance (expressed in [m]) with the corresponding model distance (expressed in [mu]).
4) Field measure check distances. Use steel table and record values between pairs of points of interest that; can be measured with a steel tape (e.g. not having to pass through solid objects); and are representative of the full 3D shape of the table
5) Compute and analyze check distance results. Evaluate distances between appropriate combinations of model points to obtain model distances in the model frame (in [mu]) for each of the field measured distances. Apply scale factor to express these the computed check distances in Ref frame units (in [m]).
6) Compare the computed check distance values with the corresponding field measured values to report differences and statistics.

Figure 9 presents the two images that form the stereo pair used for 3D object reconstruction. The image measurements visible in this figure were used as tie points for relative orientation computation, along with camera calibration values determined in section III-B.

Since the relative orientation solution immediately provides 3D coordinates for all tie points, the tie points were placed on feature locations convenient to use for check distances. The annotation in figure 10 identifies which inter-point distances are included in the check distance evaluation process.

The computed check distances, field measured check distance measurements and a comparison of the two are presented in figure 11.

Overall the 3D object reconstruction validation process is entirely consistent with estimates and expectations developed in conjunction with the camera calibration. I.e. the 9 mm table reconstruction average error magnitude compares well with the approximate 1 cm uncertainty in the measured distances used for camera calibration.

IV. Conclusions

The described experiment results demonstrate that the calibration process is effective. It is capable of providing reasonable quality approximation of a camera's principal distance values using a single photo and a few easy-to-acquire object measurements.

The precision of the results may seem poor by engineering grade photogrammetry standards which often report results with precision expressed in fractions of a pixel. However, these results are obtained from only five simple observations (two image points and three object distances) and with simple algebraic computations.

The result quality should be more than sufficient for general initialization type use such as bootstrapping high precision iterative algorithms (e.g. fully rigorous bundle adjustment methods), and likely also good enough for many applications which are satisfied with solution precision better than a percent or so.

The example calibration case involves a strong geometric configuration which immediately produces a unique solution with relatively good numeric precision. However, for weaker imaging geometries, there can be a physically real ambiguity in the computed solution values. In the weak geometry cases, the ambiguity is associated with attempting calibration when not enough information is available from a single object space angle, and generally should be avoid when practical.

For situations in which calibration must be attempted with weak imaging geometry, then additional information is necessary to obtain a unique solution. This information could come from various sources. One obvious on approach is to observe an additional angle relationship(s) within the same photo by measuring additional object distances, then identify which of the multiple solution values are in common to each case.

However, if practical camera calibration is the intended goal, then some minimal care should be taken to acquire calibration images in which the corresponding image features appear approximately on opposite sides of the image relative to the center of the image.

Overall, the described process is relatively easy. Evaluation of the precision of the computed calibration and analysis of the 3D reconstruction validation results indicate that the proposed method is effective.

References

[1] Hestenes, D., "New Foundations for Classical Mechanics", Second Ed., Springer Netherlands, 1999.
[2] Knopp, D., "Entrance Pupil Displacement Model", Stellacore document, Revised 2020.04.
[3] Knopp, D., "General Optical Distortion Model", Stellacore document, Revised 2020.04.
[4] Laurinolli, T., "What is geometric algebra", https://lyseo.edu.ouka.fi/cms7/sites/default/files/geometric_algebra-tl.pdf, Visited 2020.05.